Terahertz Spectroscopic Differentiation of Microstructures in Protein Gels

Gretel M. Png[1], Robert J. Falconer[2], Bernd M. Fischer[1,3], Hidayatul A. Zakaria[2], Samuel P. Mickan[1], Anton P.J. Middelberg[2], Derek Abbott[1]

[1]*Centre for Biomedical Engineering, School of Electrical and Electronic Engineering, University of Adelaide, Adelaide, SA 5005, Australia*
[2]*Australian Institute for Bioengineering and Nanotechnology, University of Queensland, St Lucia, QLD 4072, Australia*
[3]*French-German Research Institute of Saint-Louis (ISL), 5 rue du Général de Cassagnou, 68301 Saint-Louis Cedex, France*

gretel.png@adelaide.edu.au

Abstract: We demonstrate that terahertz (THz) spectroscopy can be used to differentiate soft protein microstructures. Differentiation of soft microstructures in gels has to date been performed using optical imaging techniques (e.g. electron microscope) and Fourier Transform Infra-Red (FTIR) spectroscopy for the mid-IR range, but a differentiation tool for the THz frequency range is lacking. Particulate and fine-stranded (fibrillar) soft protein microstructures are of interest, particularly to medical researchers, because they form from naturally occurring proteins that are thought to be involved in several human diseases, such as Alzheimer's disease. In this study, globular β-lactoglobulin structures with diameters of 2 μm, and fibrillar structures with diameters less than 0.03 μm are observed between 0.8 and 1.5 THz. Results show that the globular structures have a decline in THz transmission when compared to the fibrillar ones. The cause of this decline is possibly due to Rayleigh scattering from the globular microstructures.

OCIS codes: (300.6495) Spectroscopy, terahertz; (170.0170) medical optics and biotechnology; (120.4290) Nondestructive testing

References and links

1. A. G. Markelz, A. Roitberg, and E. J. Heilweil, "Pulsed terahertz spectroscopy of DNA, bovine serum albumin and collagen between 0.1 and 2.0 THz," Chemical Physics Letters **320**, 42–48 (2000).
2. B. M. Fischer, M. Walther, and P. U. Jepsen, "Far-infrared vibrational modes of DNA components studied by terahertz time-domain spectroscopy," Physics in Medicine and Biology **47**, 3807–3814 (2002).
3. S. E. Whitmire, D. Wolpert, A. G. Markelz, J. R. Hillebrecht, J. Galan, and R. R. Birge, "Protein flexibility and conformational state: A comparison of collective vibrational modes of wild-type and D96N bacteriorhodopsin," Biophysical Journal **85**, 1269–1277 (2003).
4. K. Siegrist, C. R. Bucher, I. Mandelbaum, A. R. H. Walker, R. Balu, S. K. Gregurick, and D. F. Plusquellic, "High-resolution terahertz spectroscopy of crystalline trialanine: Extreme sensitivity to β-sheet structure and cocrystallized water," Journal of the American Chemical Society **128**, 5764–5775 (2006).
5. A. G. Markelz, J. R. Knab, J. Y. Chen, and Y. He, "Protein dynamical transition in terahertz dielectric response," Chemical Physics Letters **442**, 413–417 (2007).
6. C. Zhang, E. Tarhan, A. K. Ramdas, A. M. Weiner, and S. M. Durbin, "Broadened far-infrared absorption spectra for hydrated and dehydrated myoglobin," Journal of Physical Chemistry B **108**, 10,077–10,082 (2004).
7. J. Knab, B. Shah, J.-Y. Chen, and A. Markelz, "Critical hydration and temperature effects on terahertz biomolecular sensing," in *Chemical and Biological Standoff Detection III*, J. O. Jensen and J.-M. Thériault, eds., Proc. SPIE **5995**, 59950P (2005).

#111526 - $15.00 USD Received 18 May 2009; revised 1 Jul 2009; accepted 1 Jul 2009; published 16 Jul 2009

8. J. Knab, J.-Y. Chen, and A. Markelz, "Hydration dependence of conformational dielectric relaxation of lysozyme," Biophysical Journal **90**, 2576–2581 (2006).
9. C. Kistner, A. Andre, T. Fischer, A. Thoma, C. Janke, A. Bartels, T. Gisler, G. Maret, and T. Dekorsy, "Hydration dynamics of oriented DNA films investigated by time-domain terahertz spectroscopy," Applied Physics Letters **90**, 233902 (2007).
10. A. G. Markelz, "Terahertz dielectric sensitivity to biomolecular structure and function," IEEE Journal of Selected Topics in Quantum Electronics **14**, 180–190 (2008).
11. S. Ebbinghaus, S. J. Kim, M. Heyden, X. Yu, M. Gruebele, D. M. Leitner, and M. Havenith, "Protein sequence- and pH-dependent hydration probed by terahertz spectroscopy," Journal of the American Chemical Society **130**, 2374–2375 (2008).
12. K. G. de Kruif, M. A. M. Hoffmann, M. E. van Marle, P. J. J. M. van Mil, S. P. F. M. Roefs, M. Verheul, and N. Zoon, "Gelation of proteins from milk," Faraday Discussions **101**, 185–200 (1995).
13. R. Mercadé-Prieto and X. D. Chen, "Dissolution of whey protein concentrate gels in alkali," American Institute of Chemical Engineers (AIChE) Journal **52**, 792–803 (2006).
14. D. J. Selkoe, "Folding proteins in fatal ways," Nature **426**, 900–904 (2003).
15. J. Näslund, V. Haroutunian, R. Mohs, K. L. Davis, P. Davies, P. Greengard, and J. D. Buxbaum, "Correlation between elevated levels of amyloid β-peptide in the brain and cognitive decline," Journal of the American Medical Association **283**, 1571–1577 (2000).
16. S. Y. Tan and M. B. Pepys, "Amyloidosis," Histopathology **25**, 403–414 (1994).
17. W. S. Gosal, A. H. Clark, and S. B. Ross-Murphy, "Fibrillar β-Lactoglobulin gels: Part 1. Fibril formation and structure," Biomacromolecules **5**, 2408–2419 (2004).
18. J. J. Resch, C. R. Daubert, and E. A. Foegeding, "β-Lactoglobulin gelation and modification: Effect of selected acidulants and heating conditions," Journal of Food Science **70**, C79–C86 (2005).
19. T. Lefèvre and M. Subirade, "Molecular differences in the formation and structure of fine-stranded and particulate β-lactoglobulin gels," Biopolymers **54**, 578–586 (2000).
20. E. A. Foegeding, P. R. Kuhn, and C. C. Hardin, "Specific divalent cation-induced changes during gelation of β-lactoglobulin," Journal of Agricultural and Food Chemistry **40**, 2092–2097 (1992).
21. H. M. Hudson, C. R. Daubert, and E. A. Foegeding, "Rheological and physical properties of derivitized whey protein isolate powders," Journal of Agricultural and Food Chemistry **48**, 3112–3119 (2000).
22. M. Verheul, J. S. Pedersen, S. P. F. M. Roefs, and K. G. de Kruif, "Association behavior of native β-lactoglobulin," Biopolymers **49**, 11–20 (1999).
23. M. E. Hines and E. A. Foegeding, "Interactions of α-lactalbumin and bovine serum-albumin with β-lactoglobulin in thermally induced gelation," Journal of Agricultural and Food Chemistry **41**, 341–346 (1993).
24. B. Y. Qin, M. C. Bewley, L. K. Creamer, H. M. Baker, E. N. Baker, and G. B. Jameson, "Structural basis of the Tanford transition of bovine β-lactoglobulin," Biochemistry **37**, 14,014–14,023 (1998).
25. E. H. C. Bromley, M. R. H. Krebs, and A. M. Donald, "Aggregation across the length-scales in β-lactoglobulin," Faraday Discussions **128**, 13–27 (2005).
26. M. R. H. Krebs, G. L. Devlin, and A. M. Donald, "Protein particulates: Another generic form of protein aggregation?" Biophysical Journal **92**, 1336–1342 (2007).
27. G. M. Kavanagh, A. H. Clark, and S. B. Ross-Murphy, "Heat-induced gelation of globular proteins: Part 3. Molecular studies on low pH β-lactoglobulin gels," International Journal of Biological Macromolecules **28**, 41–50 (2000).
28. S. I. Takata, T. Norisuye, N. Tanaka, and M. Shibayama, "Heat-induced gelation of β-lactoglobulin. 1. Time-resolved dynamic light scattering," Macromolecules **33**, 5470–5475 (2000).
29. J. I. Boye, C. Y. Ma, A. Ismail, V. R. Harwalkar, and M. Kalab, "Molecular and microstructural studies of thermal denaturation and gelation of β-lactoglobulins A and B," Journal of Agricultural and Food Chemistry **45**, 1608–1618 (1997).
30. E. H. C. Bromley, M. R. H. Krebs, and A. M. Donald, "Mechanisms of structure formation in particulate gels of β-lactoglobulin formed near the isoelectric point," European Physical Journal E **21**, 145–152 (2006).
31. C. Le Bon, T. Nicolai, and D. Durand, "Kinetics of aggregation and gelation of globular proteins after heat-induced denaturation," Macromolecules **32**, 6120–6127 (1999).
32. C. M. Bryant and D. J. McClements, "Molecular basis of protein functionality with special consideration of cold-set gels derived from heat-denatured whey," Trends in Food Science & Technology **9**, 143–151 (1998).
33. W. S. Gosal, A. H. Clark, and S. B. Ross-Murphy, "Fibrillar β-Lactoglobulin gels: Part 2. Dynamic mechanical characterization of heat-set systems," Biomacromolecules **5**, 2420–2429 (2004).
34. W. S. Gosal, A. H. Clark, and S. B. Ross-Murphy, "Fibrillar β-lactoglobulin gels: Part 3. Dynamic mechanical characterization of solvent-induced systems," Biomacromolecules **5**, 2430–2438 (2004).
35. P. C. Ashworth, J. A. Zeitler, M. Pepper, and V. P. Wallace, "Terahertz spectroscopy of biologically relevant liquids at low temperatures," in *Proceedings of Joint 31st International Conference on Infrared and Millimeter Waves and 14th International Conference on Terahertz Electronics (IRMMW-THz)* (IEEE, Shanghai, China, 2006), p. 184.
36. M. A. de la Fuente, H. Singh, and Y. Hemar, "Recent advances in the characterisation of heat-induced aggregates

#111526 - $15.00 USD Received 18 May 2009; revised 1 Jul 2009; accepted 1 Jul 2009; published 16 Jul 2009

and intermediates of whey proteins," Trends in Food Science & Technology **13**, 262–274 (2002).
37. L. N. Arnaudov and R. de Vries, "Thermally induced fibrillar aggregation of hen egg white lysozyme," Biophysical Journal **88**, 515–526 (2005).
38. P. H. Siegel, "Terahertz technology," IEEE Transactions on Microwave Theory and Techniques **50**, 910–928 (2002).
39. A. J. Fitzgerald, E. Berry, N. N. Zinov'ev, S. Homer-Vanniasinkam, R. E. Miles, J. M. Chamberlain, and M. A. Smith, "Catalogue of human tissue optical properties at terahertz frequencies," Journal of Biological Physics **129**, 123–128 (2003).
40. G. M. Png, J.-W. Choi, B. W.-H. Ng, S. P. Mickan, D. Abbott, and X.-C. Zhang, "The impact of hydration changes in fresh bio-tissue on THz spectroscopic measurements," Physics in Medicine and Biology **53**, 3501–3517 (2008).
41. C. F. Bohren and D. R. Huffman, *Absorption and Scattering of Light by Small Particles*, Wiley science paperback series (John Wiley & Sons, New York, NY, USA, 1983).
42. H. C. van de Hulst, *Light Scattering by Small Particles* (John Wiley & Sons, Inc., New York, USA, 1957).
43. E. F. Knott, J. F. Shaeffer, and M. T. Tuley, *Radar Cross Section*, The SciTech radar and defense series, 2nd ed. (SciTech Publishing Inc., Rayleigh, NC, USA, 2004).
44. H. T. Meryman, "Mechanics of freezing in living cells and tissues," Science **124**, 515–521 (1956).
45. M. Bucciantini, E. Giannoni, F. Chiti, F. Baroni, L. Formigli, J. Zurdo, N. Taddei, G. Ramponi, C. M. Dobson, and M. Stefani, "Inherent toxicity of aggregates implies a common mechanism for protein misfolding diseases," Nature **416**, 507–511 (2002).

1. Introduction

In this decade, terahertz (THz or T-ray, 0.1–10 THz) time domain spectroscopy (THz-TDS) has been applied to the study of biomolecules, namely proteins and nucleic acids. Several authors have investigated the vibrational and torsional modes, and dynamics of proteins and nucleic acids [1–5]. More recently, interest has shifted towards the structure and function of biomolecules. Terahertz-TDS has been used to investigate the phonon resonances in three dimensional (3D) crystalline lattices of small organic molecules (polypeptides and polynucleotides) in various states: denatured, native, hydrated and dry [6–9]. Results show that THz absorption is affected by molecular conformation [10]. In addition, THz-TDS has been linked to solvation free energy changes induced by protein folding in bacteriophage λ_{6-85} [11]. This finding implies that THz spectroscopy has the potential to indirectly probe protein folding through the examination of induced changes in the protein's hydration shell.

The influence of molecular conformation has led us to explore whether THz spectroscopy can be used to probe uniform microstructures in biological materials. Soft (semi-rigid) microstructures formed by folding and aggregation in proteins are common in nature and in artificial environments. For example, the formation of protein-based 3D soft microstructures has been exploited in the preparation of food products such as cheeses and yogurt [12]. Protein-based 3D soft microstructures are also a type of contaminant in the dairy industry [13]. In humans, the formation and accumulation of unnaturally large numbers of soft protein microstructures in bio-tissue can cause degenerative diseases such as Alzheimer's and Parkinson's [14–16]. The widespread use and occurrence of protein-based soft microstructures make them ideal as a new class of biomaterials to be investigated with THz.

The study of soft microstructures is currently limited due to the destructive nature of available investigative tools. For example, staining has been used to detect specific bonds, such as intermolecular β-pleated sheet interactions [17], whereas electron microscopy has been used to visualize microstructures [17, 18]. Non-destructive Fourier Transform Infra-Red (FTIR) spectroscopy has been used to study soft microstructures but only in the mid-IR range [19]. Soft microstructures therefore present an interesting analytical challenge for non-destructive THz spectroscopy.

In this study, we demonstrate novel THz spectroscopic differentiation of three protein microstructures: globular, fine fibrillar, and coarse fibrillar. Our spectroscopic measurements of thermally induced protein gels show that the type of protein microstructure has a direct influ-

#111526 - $15.00 USD Received 18 May 2009; revised 1 Jul 2009; accepted 1 Jul 2009; published 16 Jul 2009

ence on the measured THz absorption property.

2. β-Lactoglobulin Gels

When casein micelles are removed from skimmed bovine milk, the colloidal liquid that remains is whey protein. Commercial whey protein is available either as whole whey protein isolate (WPI) powder, or separated into its protein constituents: 68% β-lactoglobulin, 17% α-lactalbumin, 7% bovine serum albumin, and 7% immunoglobulin G [20]. β-Lactoglobulin and WPI are most often used in thermal gelation studies conducted by the food industry [12, 21].

Bovine β-lactoglobulin (or β-lg) exists either in its native form, or as one of two variants (β-lg A and B). The native form is used in this study. β-Lactoglobulin is so named because it has a secondary structure of antiparallel β-pleated sheets [22] as shown in Fig. 1(a). When β-lg is heated above 65–70°C in a solution environment, one of several possible chemical processes occurs depending on the acidity of the solution environment [23]. Two examples—fibrillar and globular—are shown in Fig. 1(b). The heating and chemical change in β-lg, called thermal gelation, results in the production of β-lg gel.

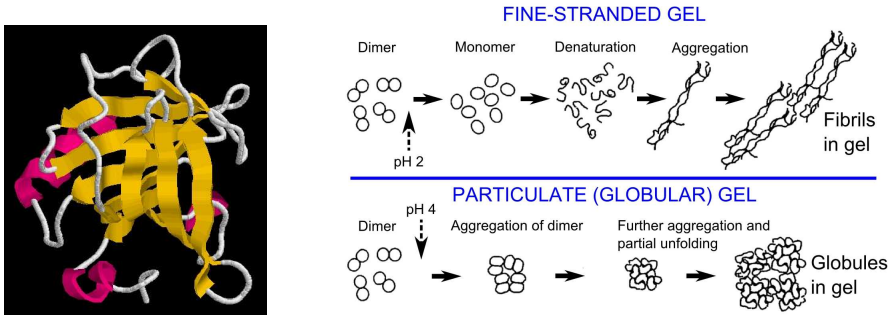

(a) Native β-lg molecule (b) Formation of fibrillar and globular gels

Fig. 1. (a) Cartoon diagram of a β-lg molecule obtained from the Protein Data Bank (PDB), and rendered using Rasmol (PDB ID: 1BSY). This molecule is colored according to its secondary structures: eight antiparallel β-pleated sheets (yellow), α-helix segments (magenta), and other residues (white). After [24]; (b) Succession of steps leading to the formation of fibrillar and globular β-lg gels in a solution environment at $>$ 65–70°C. The process starts off with β-lg dimers (a dimer contains two β-lg molecules, each with structure as shown by the cartoon diagram on the left). Depending on the acidity of the solution environment, the dimer aggregates to form either fine fibrils (pH 2) or globules (pH 4). Coarse fibrils are formed at pH 7. Adapted from [19].

2.1. Influence of pH on Microstructure Formation in Gels

The isoelectric point (pI) of a protein is the pH value at which there is no net electrical charge on each individual protein molecule. For β-lg, the pI is reported to be between pH 4.8 and 5.1 [25, 26]. When β-lg protein is immersed in an aqueous environment, the acidity of this environment can be manipulated to be close to or away from β-lg's pI, resulting in a change in the net charge on each individual protein molecule. For example, at pH 2 the net charge is +20 (unitless); as illustrated in Fig. 1(b), this large net charge affects the oligomerization process in β-lg such that more monomers than dimers exist [22, 25]. This oligomerization condition, which also exists above pH 6 [27], favors the formation of fibrillar microstructures during thermal gelation. Furthermore, the presence of large numbers of β-lg monomers causes the β-lg solution to appear visually clear at pH values away from its pI, which is between pH 4.8 and 5.1 as highlighted above.

#111526 - $15.00 USD Received 18 May 2009; revised 1 Jul 2009; accepted 1 Jul 2009; published 16 Jul 2009

Conversely, when the pH of the solution is close to the pI, there is only a small net charge on each molecule; as illustrated in Fig. 1(b), the small net charge results in the presence of more dimers than monomers after oligomerization. These dimers can also associate to form larger oligomers called octamers [22]. This condition favors the formation of globular microstructures during thermal gelation. Additionally, the presence of large numbers of β-lg dimers causes the β-lg solution to appear turbid at pH values close to its pI.

Examples of fibrillar and globular microstructures are presented in Figs. 2(a)–2(c). There is a clear visual distinction between fibrillar and globular microstructures: globular microstructures resemble balls whereas fibrils resemble strands. Fibrils synthesized at pH 2 are fine and "worm-like" whereas those synthesized at pH 7 are coarser. Coarse fibrils are much thicker than fine fibrils, being $\sim$30 nm in diameter whereas fine fibrils are $\sim$4 nm in diameter [28]. Coarse fibrils also tend to form tight clumps [25]. The size of globular microstructures has been reported by several authors as being between 100 nm and 2 μm [18, 26, 29, 30]. The large variation in diameters is due to different heating conditions used by each author; in this study, our heating condition produces globules with diameters of 2 μm.

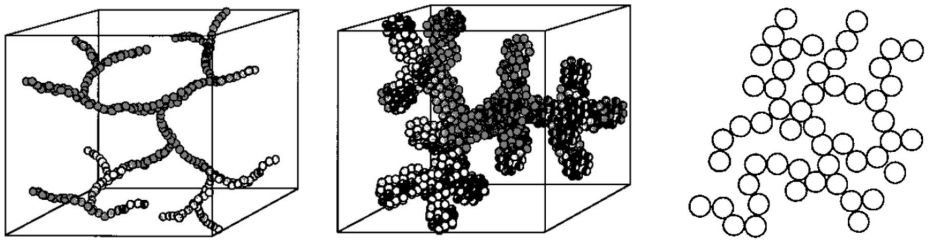

(a) Schematic representation of pH 2 gel microstructure

(b) Schematic representation of pH 7 gel microstructure

(c) Schematic representation of pH 4 gel microstructure

Fig. 2. (a and b) At pH 2, the β-lg monomers form chains that look "worm-like", being typically between 100–200 nm in length and $\sim$4 nm in diameter. Alternatively at pH 7, the β-lg monomers tend to stick to each other, resulting in fractal aggregate formation. The fibrils also look "worm-like" but are thicker than the ones seen at pH 2, being typically $\sim$30 nm in diameter. After [17, 28]; (c) This schematic of pH 4 globules is not drawn to the same scale as the figures to the left. The globules clearly resemble balls with diameter that varies with the rate of heating. Diameters reported in literature vary between 100 nm and 2 μm. After [30, 31].

The protein microstructures in β-lg gel have a semi-rigid nature due to *(i)* covalent bonds linked by intermolecular disulphide bonds, *(ii)* intermolecular β-pleated sheets interactions held together by multiple hydrogen bonds, and *(iii)* hydrophobic interactions [32]. The acidity of the solution environment during thermal gelation alters the strength of the bonds and interactions, creating the different types of microstructures mentioned above. β-Lactoglobulin gels can therefore be synthesized with desired microstructures by manipulating the acidity and temperature of the solution environment [19, 25]. Microstructures synthesized at pH 2 (fine fibrils), pH 4 (globules) and pH 7 (coarse fibrils) are most commonly encountered in literature, thus they are investigated in this study.

3. Synthesizing β-Lactoglobulin Gels

The synthesis, gelation dynamics and kinetics of β-lg gels are discussed in detail in [17, 18, 33, 34] and references therein. A summary of the steps taken to synthesize gels is as follows. Fifteen percent (weight/volume or w/v) of β-lg (Sigma-Aldrich, L0130) is dissolved in 20 mM, pH 7 phosphate buffer. The protein mixture is then filtered with a 0.2 μm syringe filter to yield

#111526 - $15.00 USD Received 18 May 2009; revised 1 Jul 2009; accepted 1 Jul 2009; published 16 Jul 2009

an optically clear solution. The pH is adjusted to 7.0, 4.0 and 2.0 with 1 M HCl. As highlighted in Section 2.1, the solution at pH 2 and 7 is clear whereas it is turbid at pH 4 (close to the pI: pH 4.8–5.1).

One milliliter of solution is dispensed into an epoxy-sealed polycarbonate petri dish, and then laid flat at 80°C for 3 hours to induce thermal gelation. The sealed dish prevents the gel from dehydrating during heating, ensuring consistent water content in all samples. As highlighted in Section 2.1, the size of the globules in the pH 4 gel is sensitive to the heating conditions, thus the same heater and heat settings have been used in this study to ensure consistency in our samples.

After heating, the gel is allowed to cool at room temperature. The pH 2 and 7 gels appear clear, indicating uniform gel formation; pH 4 gel appears turbid due to the globular nature of the microstructures. When cooled, the gels are frozen at -20°C. Freezing is necessary because the gel holds water [21]. Since ice is more transparent than liquid water in the low THz (0.1–3 THz) frequency range [35], THz measurement of frozen gel (as opposed to that of non-frozen gel) will demonstrate improved dynamic range and bandwidth. All gels appear turbid when frozen as shown by the optical image of a frozen pH 2 gel in Fig. 3.

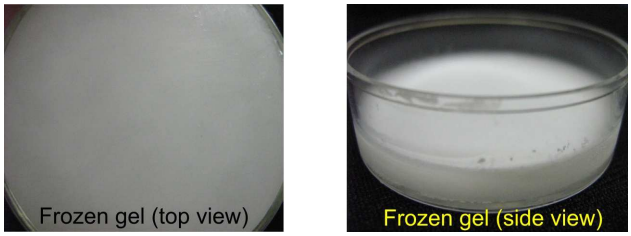

Fig. 3. Frozen pH 2 gel shown here as an example of the appearance of the gels. All the frozen gels appear turbid and opaque. For illustrative purpose, the frozen gel on the right is shown in its dish but without the sealed lid.

The temperature of the gels is further reduced to 123 K (-150°C) before measurements are made; the reason for choosing this temperature is discussed in Section 5.2. In order to measure the gels at this temperature, it is necessary to use a cryostat together with the THz system. The cryostat requires vacuum pumping in order to achieve low temperatures below 247 K. To prevent the gels from lyophilizing (freeze-drying) in this environment, the gels are measured *in situ* in their sealed dishes.

Since the sealed petri dishes are not resealable once opened, it is not possible to directly measure a gel's thickness without sacrificing it. Measurement of a gel's thickness cannot be made externally from the outside of the dish because of the meniscus effect along the wall of each petri dish. Consequently, thickness measurements are performed only after the samples have been probed with THz radiation, whereby the lids of the dishes are broken to access the gels.

Minimal handling of the frozen gels is critical to prevent thawing during thickness measurements. The use of a graduated rule allows fast and accurate measurements with minimal handling of the dishes. The rule is inserted into several positions in each dish in order to average the thickness of the sample. This process is repeated with several different batches of gels so as to obtain the overall average thickness of all frozen gels, which is 0.7 mm$\pm$0.1 mm.

3.1. Synthesizing β-Lactoglobulin Solutions

β-Lactoglobulin solutions differ from β-lg gels in that they are not heat treated, thus thermal gelation does not occur. This means that β-lg solutions do not contain microstructures. The only two differences between the pH 2, 4 and 7 solutions are their acidity, and the turbidity of

#111526 - $15.00 USD Received 18 May 2009; revised 1 Jul 2009; accepted 1 Jul 2009; published 16 Jul 2009

the pH 4 solution (the reason for its turbidity is explained in Section 2.1).

The β-lg solutions are synthesized at the same time as the gels, and frozen at -20°C. When frozen, the pH 2 and 7 solutions appear glassy, while the pH 4 solution remains turbid. Prior to measurements, the temperature of the solutions are also further reduced to 123 K (-150°C). Like the gels, access to the solutions for the purpose of measuring their thickness is not possible due to the sealed dishes, thus thickness measurements are also only performed after the samples have been probed with THz radiation. The thickness of frozen solution is found to be 0.7 mm$\pm$0.1 mm after averaging over several different batches of solutions. This similarity in thickness to the gel is expected since the same volume of liquid is used per dish. The presence of microstructures in the gel should not influence its thickness since the microstructures are too small to cause a difference in the sub-millimeter resolution used for measuring thickness in this study.

Results from THz measurements of both the gels and solutions at 123 K are presented in Section 5.

3.2. Verifying Microstructures in Gels used in this Study

The gels manufactured in this study are examined with an electron microscope to confirm that microstructures exist. As shown in Fig. 4, the gel structures observed in our study are not random accumulations of fibrils and globules but rather are well-organized, fixed 3D structures consistent with those reported elsewhere [17, 18, 26, 36, 37]; the pH 2 gel has uniform fibrillar structure, the pH 7 gel has a uniform 3D matrix, and the pH 4 gel has a 3D globular matrix. Additionally, Thioflavin T dye tests on the gels confirm the presence of β-pleated sheets in both the fibrillar and globular gels, confirming that the gels synthesized in this study are consistent with those reported in literature. In summary, we have synthesized three gels with identical chemical composition but distinctly different microstructures.

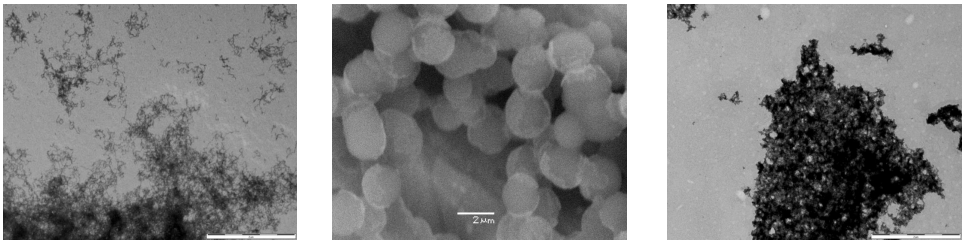

(a) pH 2 gel: fine fibrillar aggregates (b) pH 4 gel: globular aggregates (c) pH 7 gel: coarse fibrillar aggregates

Fig. 4. Electron micrographs of the gels synthesized in this study. The white scale bar at the bottom of each figure represents 2 μm. (a) Transmission electron micrograph (TEM) of pH 2 gel reveals fine fibrillar aggregates that are scattered loosely throughout the gel; (b) Scanning electron micrograph (SEM) of pH 4 gel reveals globular aggregates that cluster to form layers of balls; (c) TEM of pH 7 gel also reveals the presence of fibrillar aggregates but these fibrils are coarser than those at pH 2. Like the pH 4 globules, the pH 7 fibrils also cluster to form clumps.

4. Terahertz Spectroscopic Measurements

This study utilizes two different transmission-mode THz-TDS systems based on the generation of THz pulses using an ultrafast (90 fs) near-infrared laser (Spectra-Physics Mai Tai). One system is the commercial T-ray-2000 from Picometrix, which consists of a pair of fiber-optic coupled THz emitter and detector heads as shown in Fig. 5. The other THz-TDS system—the custom photoconductive antenna (PCA) system—utilizes GaAs PCAs for THz generation and coherent detection (Fig. 6). Further details of a typical THz-TDS system are found in [38].

#111526 - $15.00 USD Received 18 May 2009; revised 1 Jul 2009; accepted 1 Jul 2009; published 16 Jul 2009

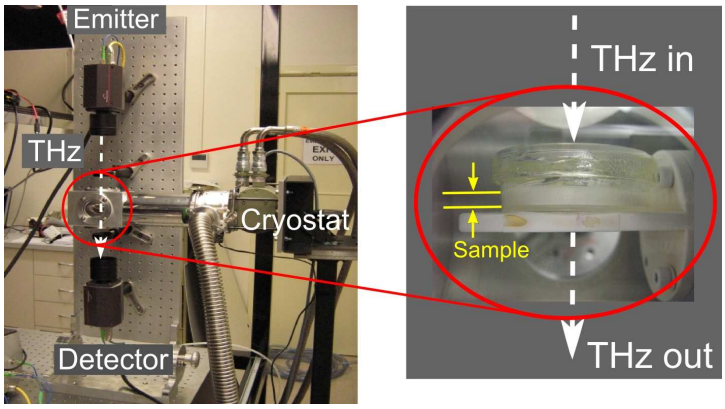

Fig. 5. The Picometrix T-ray-2000 system used in this study, shown without the nitrogen-purged chamber. The upright arrangement of this system allows the dishes to be mounted quickly and easily on a horizontal platform without the need for clamps. A hole in the platform is wide enough to allow unobstructed THz transmission through the sample.

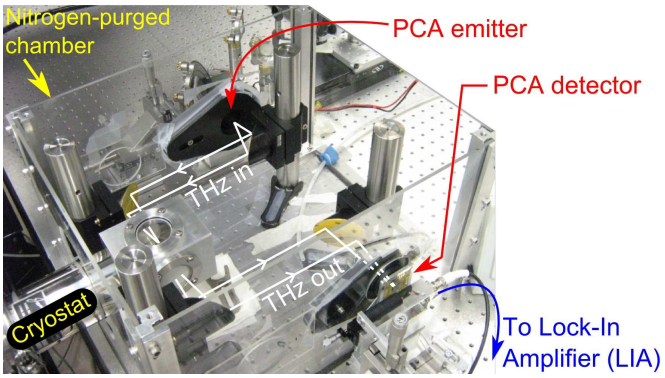

Fig. 6. The custom PCA system used in this study, shown with its nitrogen-purged chamber. The THz beam propagates in a path that is parallel to the optical bench, thus the samples are mounted perpendicular to the optical bench (unlike the case for the Picometrix system).

A closed-cycle cryostat (Janis CCS-450) enclosed inside a nitrogen-purged chamber is used to keep the samples frozen during measurements. The samples are mounted inside the cryostat as shown in Fig. 5. Since the samples are sealed as described in Section 3, humidity and temperature are consistent across the measurements, thus reducing uncertainties caused by variations in the laboratory environment.

Since the samples are measured *in situ* in sealed dishes, the reference signal $E_{\text{ref}}(t)$ is the transmitted THz signal through an empty sealed dish, and $E_{\text{sample+ref}}(t)$ is the transmitted THz signal through a sample and its sealed dish. Fourier transforms of $E_{\text{ref}}(t)$ and $E_{\text{sample+ref}}(t)$ give $E_{\text{ref}}(\omega)$ and $E_{\text{sample+ref}}(\omega)$ respectively, with magnitude and phase components as follows:

$$E_{\text{ref}}(\omega) = |E_{\text{ref}}(\omega)|\, e^{(-i\omega t + \phi_{\text{ref}}(\omega))} \quad (1)$$

$$E_{\text{sample+ref}}(\omega) = |E_{\text{sample+ref}}(\omega)|\, e^{(-i\omega t + \phi_{\text{sample+ref}}(\omega))} \quad (2)$$

$$|E_{\text{sample}}(\omega)| = \left| \frac{E_{\text{sample+ref}}(\omega)}{E_{\text{ref}}(\omega)} \right| \quad (3)$$

$$\phi_{\text{sample}}(\omega) = \phi_{\text{sample+ref}}(\omega) - \phi_{\text{ref}}(\omega)\,, \quad (4)$$

#111526 - $15.00 USD Received 18 May 2009; revised 1 Jul 2009; accepted 1 Jul 2009; published 16 Jul 2009

where ω denotes the angular frequency.

A sample's refractive index $n(\omega)$ and extinction coefficient $\alpha(\omega)$ in the THz frequency range can be calculated by substituting Eqs. (3) and (4), and the sample's thickness d into the equations below:

$$n_{\text{sample}}(\omega) = \frac{c\,\phi_{\text{sample}}(\omega)}{\omega\, d} + 1 \tag{5}$$

$$\alpha_{\text{sample}}(\omega) = -\frac{2}{d}\ln\left(\frac{|E_{\text{sample}}(\omega)|\,[1+n_{\text{sample}}(\omega)][n_{\text{dish}}(\omega)+n_{\text{sample}}(\omega)]}{2n_{\text{sample}}(\omega)[1+n_{\text{dish}}(\omega)]}\right), \tag{6}$$

where c is the speed of light *in vacuo*, and $n_{\text{dish}}(\omega)$ is the refractive index of the epoxy-sealed polycarbonate petri dish used to house each sample.

Analysis of a sample's refractive index is necessary to ascertain if dispersion occurs inside the sample. If the profile of the refractive index is relatively flat over the frequencies of interest, then there is negligible dispersion in the material. The extinction coefficient provides a gauge of the strength of the detected THz signal. If extinction is high, then the test material absorbs and/or scatters the incident THz signal, resulting in a weaker detected signal. Resonant frequencies of biomolecules manifest as peaks in the extinction coefficient plot, thus the extinction coefficient also helps in the identification of biomolecules. The slope of an extinction coefficient plot is another technique for differentiating between more complex biological systems such as gels and bio-tissue [39, 40].

4.1. Rayleigh Scattering

In this study, Eq. (6) is referred to as "extinction" instead of "absorption" because scattering is taken into account as being one of the contributors towards an increase or decrease in the measured THz signal strength. Extinction is therefore the sum of absorption in the material, and scattering from the material [41].

Given the small dimensions of the fibrils and globules in the gels compared to the THz wavelengths of interest in this study (wavelength λ = 750 μm–192 μm), Rayleigh scattering would be the dominant scattering encountered in our experiments. Rayleigh scattering is a special case of Mie scattering for small particles with size $\ll \lambda$. It is conventionally reported in terms of the scattering cross section (analogous to radar cross section or echo area) which is a measure of power scattered in a given direction when incident radiation illuminates a target object [41–43]. When the scattering cross section C_{sca} is normalized by the geometric cross section, the result is the scattering efficiency Q_{sca}. As given in [41], the equations describing the Rayleigh scattering efficiencies for L spheres, each with radius r, are:

$$Q_{\text{sca}}(\omega) = \frac{8Lx^4}{3}\left|\frac{m^2-1}{m^2+2}\right|^2 \tag{7}$$

$$\text{where } m(\omega) = \frac{\hat{n}_{\text{microstructure}}(\omega)}{\hat{n}_{\text{surrounding medium}}(\omega)} \tag{8}$$

$$x(\omega) = \frac{2\pi\hat{n}_{\text{microstructure}}(\omega)\,r}{\lambda} \tag{9}$$

$$\hat{n}_{\text{microstructure}}(\omega) = n_{\text{microstructure}}(\omega) + i\,\kappa_{\text{microstructure}}(\omega) = n_{\text{microstructure}}(\omega) + i\,\frac{\alpha_{\text{microstructure}}(\omega)\,c}{2\omega}, \tag{10}$$

where $n_{\text{microstructure}}(\omega)$ and $\alpha_{\text{microstructure}}(\omega)$ are averages of the experimental values $n_{\text{sample}}(\omega)$ and $\alpha_{\text{sample}}(\omega)$ respectively. In our models, we assume that the protein microstructure are suspended in air, hence $\hat{n}_{\text{surrounding medium}}(\omega) = \hat{n}_{\text{air}}(\omega) = 1.0003 \approx 1$. Since our models treat the gels as homogeneous media suspended in air, they are only approximations of the actual samples which contain more complex protein microstructures suspended in frozen solution.

#111526 - $15.00 USD Received 18 May 2009; revised 1 Jul 2009; accepted 1 Jul 2009; published 16 Jul 2009

If the incident THz radiation field is parallel to the long axis of an infinitely long cylinder, then the equations in [41] that describe Rayleigh scattering efficiencies for P infinite cylinders, each with radius r are:

$$Q_{sca}(\omega) = \frac{2P}{x}\left[|b_0(\omega)|^2 + 2|b_1(\omega)|^2\right] \quad (11)$$

$$\text{where } b_0(\omega) \approx \frac{-i\pi x^2(m^2-1)}{4} \quad (12)$$

$$b_1(\omega) \approx \frac{-i\pi x^4(m^2-1)}{32}. \quad (13)$$

Note that Eqs. (7) and (11) assume that scattering from multiple particles is a cumulative effect of scattering from individual particles, and that there is no coupling or multipath scattering between particles.

5. Results

The results in this study are presented as plots of the samples' THz extinction $\alpha(\omega)$ and refractive indices $n(\omega)$ over the usable frequency bandwidth of the systems, which spans from 0.4 to 1.56 THz. As defined in Eqs. (1–6), each $\alpha(\omega)$ or $n(\omega)$ plot presented is derived from $E_{\text{sample+ref}}(t)$ and $E_{\text{ref}}(t)$ that are each averaged over 25 measurements. Measurements are made only after the desired temperature in the cryostat has stabilized for 15 minutes. Since similar results are observed in both the Picometrix and custom PCA systems, only the Picometrix results are presented here.

5.1. *Differentiation of Structures*

The THz extinction coefficients $\alpha(\omega)$ of the pH 2, 4 and 7 gels at 123 K (-150°C) are shown in Fig. 7(a); $\alpha(\omega)$ of the pH 2, 4 and 7 solutions at the same temperature are shown in Fig. 7(b).

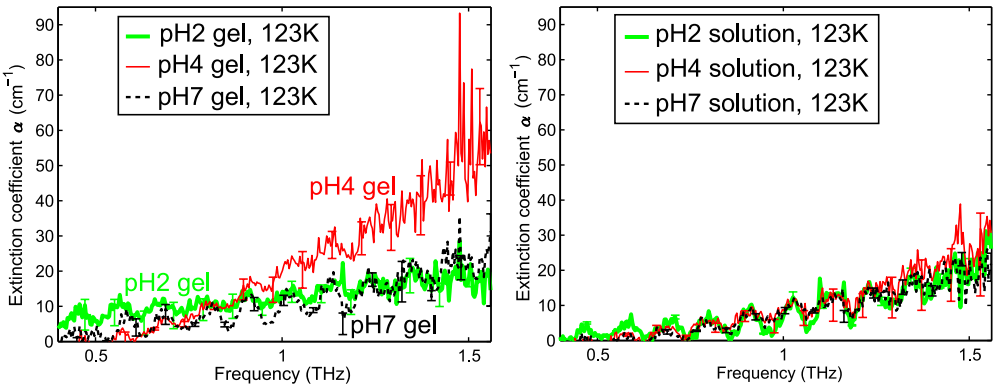

(a) THz extinction coefficients of gels at pH 2, 4 and 7 (b) THz extinction coefficients of solutions at pH 2, 4 and 7

Fig. 7. The distinct rise in the THz extinction coefficient of pH 4 gel is likely due to the globular microstructure in the gel. The two different fibrillar structures in the pH 2 and 7 gels are indistinguishable from each other. Furthermore, the fibrils have the same THz response as the solutions, which lack any microstructures.

As seen in Fig. 7(a), the gradients of all three gel plots are similar in the lower THz range, but a distinct linear rise from the baseline occurs for the pH 4 gel from ~0.8 THz onwards. For the solutions, Fig. 7(b) shows that all three solutions have similar $\alpha(\omega)$ profiles which do not deviate from the baseline. The linear rise in the $\alpha(\omega)$ profile of pH 4 gel is therefore distinct

#111526 - $15.00 USD Received 18 May 2009; revised 1 Jul 2009; accepted 1 Jul 2009; published 16 Jul 2009

from the profiles of all solutions and the pH 2 and 7 gels. Note that similar results are observed in both the Picometrix and custom THz-TDS systems.

The refractive indices of the gels and solutions are presented in Figs. 8(a) and 8(b) respectively. As apparent from these figures, the refractive index profiles of both the gels and solutions are relatively flat over the system bandwidth, indicating that there is no dispersion of the THz signal inside the samples. This means that the steep rise in THz extinction characteristic observed in the pH 4 gel is not an artifact caused by dispersion.

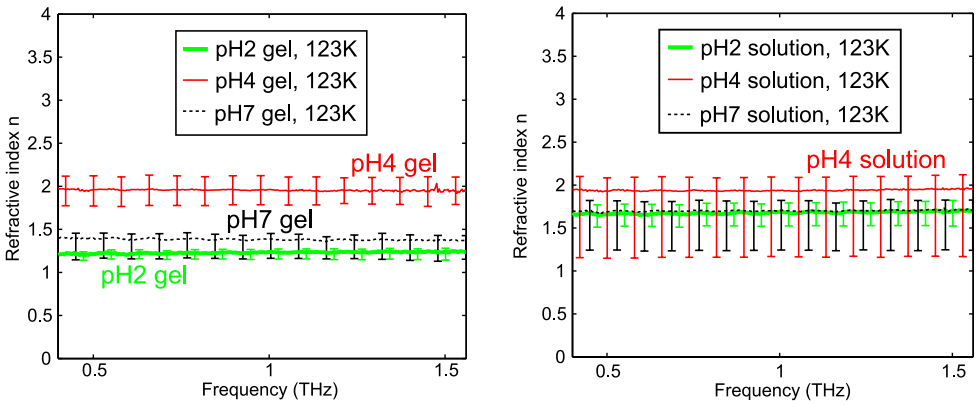

(a) Refractive indices of gels at pH 2, 4 and 7

(b) Refractive indices of solutions at pH 2, 4 and 7

Fig. 8. The refractive indices $n(\omega)$ of both the gels and solutions do not vary much with frequency since their profiles are relatively flat over the system bandwidth. This means that there is no evidence of dispersion of the THz signal inside the samples. The error bars are generated based on $\pm$ 0.1 mm uncertainty in the measurement of sample thickness.

The error distribution of the solutions' refractive indices is large when compared to those of the gels', making refractive index an unreliable parameter for distinguishing between gels and solutions. However among the gels, the refractive index of the pH 4 gel is clearly higher than those of the pH 2 and 7 gels, but this difference is not as significant as that seen in the extinction coefficient $\alpha(\omega)$.

The steep rise in the extinction coefficient of the pH 4 gel could be explained through analysis of Rayleigh scattering from spherical and cylindrical scatterers that model the globular and fibrillar microstructures respectively. As discussed in Section 2, the ball-like structures are much larger than the fibrils in the pH 2 and 7 gels, hence they appear as spherical scatterers to the incident THz radiation. Figure 9(a) presents a comparison of the Rayleigh scattering efficiencies $Q_{sca}(\omega)$ against the extinction coefficients $\alpha(\omega)$ of pH 4 and 7 gels. Equations (7) and (11) are used to generate the $Q_{sca}(\omega)$ plots based on the following parameters: radius = 1 μm for a sphere (to model a pH 4 globule); radius = 15 nm and length = 2 μm for a wide cylinder (to model a pH 7 coarse fibril). Approximately $P = 2963$ cylinders will fit into $L = 1$ sphere. The parameter P is necessary because scattering from one cylinder with the given dimensions is several orders smaller than that from one sphere, making it difficult to compare the extent of scattering on the same scale.

Although these Rayleigh scattering models for pH 4 and 7 gels are only approximations to the more elaborate microstructures in the gels, there is good agreement between the models and the experimental results. This therefore suggests that THz scattering is a possible mechanism for the observed differences in the extinction coefficient of the globular and fibrillar gels. However, when Fig. 7(a) is compared with Fig. 7(b), it might be argued that the profile of the pH 7 gel is not due to scattering by the fibrils but could be due to absorption of the solution, or scattering by

#111526 - $15.00 USD Received 18 May 2009; revised 1 Jul 2009; accepted 1 Jul 2009; published 16 Jul 2009

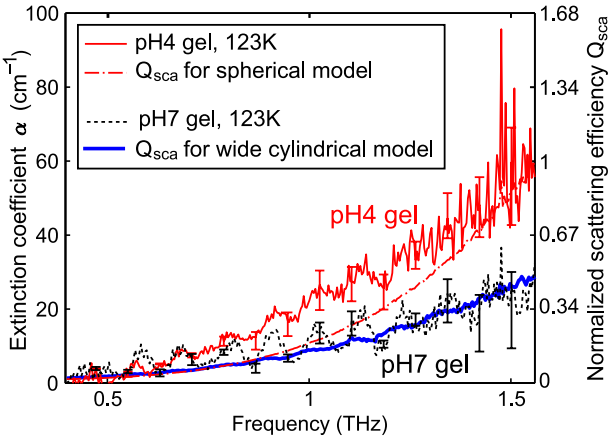

(a) Comparison of pH 4 and 7 gels' extinction coefficients and normalized Rayleigh scattering efficiencies $Q_{sca}(\omega)$

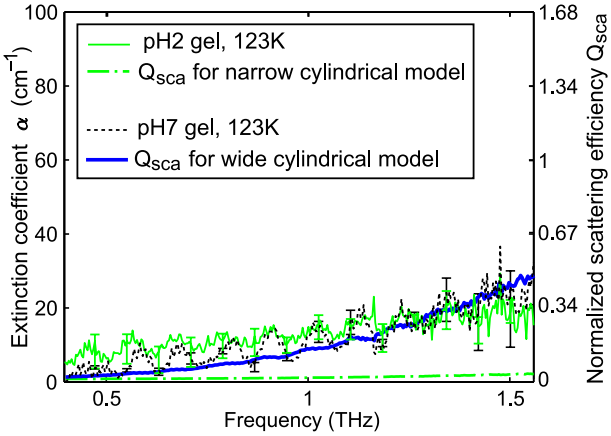

(b) Comparison of pH 2 and 7 gels' extinction coefficients and normalized Rayleigh scattering efficiencies $Q_{sca}(\omega)$

Fig. 9. Rayleigh scattering efficiencies $Q_{sca}(\omega)$ versus extinction coefficients $\alpha(\omega)$ of fibrils and globules. Rayleigh scattering is a special case of Mie scattering, and is applicable in this study due to the small dimensions of the microstructures. (a) The plot of $Q_{sca}(\omega)$ for a single sphere model of a pH 4 globule, and the plot of $Q_{sca}(\omega)$ for clusters of wide cylinders modeling the pH 7 coarse fibrils reveal that the steep rise in the extinction coefficient of the pH 4 gel could be due to scattering; (b) There is good agreement between $Q_{sca}(\omega)$ for clusters of wide cylinders and the extinction coefficient of the coarse fibrils at pH 7, but no agreement between $Q_{sca}(\omega)$ for clusters of narrow cylinders and the extinction coefficient of fine fibrils at pH 2. This indicates that the existing resolution of a THz-TDS system is insufficient for differentiating between the fine and coarse fibrils.

ice. Therefore this preliminary result motivates future experiments to further explore the effect of scattering.

For the pH 2 gel, parameters used in Eq. (11) are: radius = 2 nm, length = 2 μm for a narrow cylinder (to model a pH 2 fine fibril). Approximately $P = 166700$ narrow cylinders will fit into $L = 1$ sphere. The extinction coefficients of the pH 2 and 7 gels and solutions appear very similar over our system bandwidth, however as shown in Fig. 9(b) plots of $Q_{sca}(\omega)$ reveal that the scattering efficiencies are dissimilar. It can therefore be concluded that the fine and coarse

#111526 - $15.00 USD Received 18 May 2009; revised 1 Jul 2009; accepted 1 Jul 2009; published 16 Jul 2009

fibrillar structures in pH 2 and 7 gels respectively are too small to be differentiated given the existing resolution of a THz-TDS system.

In summary, the distinct change in the extinction coefficient of the globular aggregate as compared to the negligible change for the fibrillar aggregates strongly indicates that THz-TDS can be employed as an effective non-destructive inspection tool for differentiating between globular and fibrillar microstructures in gels, but is ineffective at differentiating between coarse and fine fibrillar microstructures.

5.2. Influence of Sample Preparation and Measurement Conditions

To ensure our results are not biased by experimental conditions, our study now explores the effects of preparation techniques, measurement temperature, and type of test media on our findings.

The first issue addressed is the influence of freezing rate. Although ice is more transparent than liquid water in the THz frequency range, large ice crystals may still scatter THz radiation and cause a decrease in the measured THz signal. Furthermore, large ice crystals may destroy the 3D microstructure in protein gels. The size of ice crystals is related to the rate of cooling [44]. The freezing process in a laboratory freezer, such as the one used in this study, is considered "slow", implying that large ice crystals are grown. Smaller ice crystals are grown through "rapid" freezing in cryogens, such as liquid nitrogen, propane and isobutane.

A separate batch of pH 4 gels and solutions is synthesized according to the steps detailed in Section 3 but is rapid frozen instead of slow frozen. The rapid frozen gels and solutions are then measured with THz in the same manner as the slow frozen samples (i.e. *in situ* in petri dishes). Results reveal that the extinction coefficients $\alpha(\omega)$ of slow and rapid frozen samples are similar, indicating that freezing rate has no observable effect on the differing extinction coefficients seen in Section 5.1 for the pH 4 gels and the other samples.

The next issue addressed is the influence of the sample holder. Since the gels and solutions are measured *in situ* in petri dishes, etalon reflections in the dishes are evident as oscillatory artifacts in the plots shown in Fig. 7. To eliminate the influence of the dishes and any other possible interference that may arise from the synthesis (e.g. air gaps between sample and dish, cracks, random ice crystals in the path of the THz beam), the pH 4 gels and solutions are lyophilized (freeze-dried) for 24 hours. Lyophilization reduces water from the sample, leaving only a small amount of bound water. The lyophilized samples therefore have a powdered texture and can be pressed into pellets for measurement with THz. In this study, the lyophilized samples are mixed with polyethylene powder to create sufficient bulk for making pellets. The thickness of the pellets is 0.62 mm $\pm$ 0.03 mm, and measurements are made at 120 K.

Results of the extinction coefficients $\alpha(\omega)$ of pH 4 pellets reveal that pH 4 gel experiences stronger THz extinction than pH 4 solution, however this difference is not as pronounced as that seen in Section 5.1 for the frozen gels and solutions that are measured *in situ* in dishes.

The final issue addressed is the influence of measurement temperature. As shown in Fig. 10, a reduction in temperature results in the reduction of the extinction coefficient $\alpha(\omega)$ of pH 4 gel. The extent of reduction in $\alpha(\omega)$ is initially large at higher temperatures (e.g. from 250 K to 220 K), but stabilizes at low temperatures. This phenomenon can be explained by the reduction in the extinction coefficient of ice at low temperatures [35]; water activity at higher temperatures results in stronger attenuation of the incident THz signal. It is therefore important to identify a temperature at which measurements are stable.

The cryostat used in our study can be cooled down to 4 K (-269°C) but the cooling time required to attain this extremely low temperature results in extended experimental time. As evident from the 120 K and 20 K plots in Fig. 10, the bandwidth and dynamic range of the measurements are similar at these two temperatures, hence measurements at extremely low

#111526 - $15.00 USD Received 18 May 2009; revised 1 Jul 2009; accepted 1 Jul 2009; published 16 Jul 2009

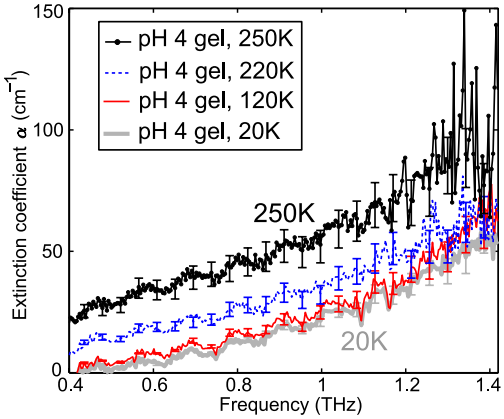

Fig. 10. The frequency bandwidth and dynamic range of the pH 4 gel measurements improve with decreasing temperatures, but begin to convergence at 180 K. There is no significant difference between the measurements made at 120 K and 20 K.

temperatures, such as 20 K, are superfluous. Measurements in this study are conducted at 123 K (-150°C), thus the observation for pH 4 gel seen in Section 5.1 is not due to water/ice activity or temperature fluctuations, but is more likely due to scattering.

6. Conclusion

In this study, we have demonstrated that THz-TDS can be used at low temperatures as a non-destructive differentiation tool for microstructures in gels derived from whey protein. Three dimensional globular (pH 4.0) and fibrillar (pH 2.0 and 7.0) microstructures have been synthesized via thermal gelation of β-lg solution at different pH values. When examined between 0.8 and 1.5 THz, the globular β-lg structures with diameters of 2 μm have a decline in transmission (rise in extinction coefficient) when compared to fibrillar structures with diameters less than 0.03 μm. The decline in transmission for the globular β-lg structures is attributed to Rayleigh scattering. Globular and fibrillar microstructures are shown to have distinct gradients of the extinction coefficients; this relative differences provides a good means of differentiating between both microstructures. The best results are obtained for frozen protein gels with lyophilized pH 4 gels showing a less pronounced change. This change in extinction coefficient for globular microstructures compared to fibrillar microstructures is shown to be independent of temperature, freezing rate and type of sample holder.

One potential application of this work is the morphological study of highly cytotoxic granular protein aggregates with THz-TDS. Such granular protein aggregates can form fibrillar aggregates that are classified as amyloid fibrils, which are believed to be responsible for the degenerative diseases mentioned in Section 1 [45]. Our future work will explore this avenue in addition to improving sample preparation and spectroscopic techniques with the aim of differentiating between fibrillar structures with different diameters.

Acknowledgments

This work was funded by the Australian Research Council (ARC) grant number DP0773111. We would like to thank Yuan Yuan Fan for assistance with the electron microscopy.

#111526 - $15.00 USD Received 18 May 2009; revised 1 Jul 2009; accepted 1 Jul 2009; published 16 Jul 2009